Challenges in Fault Detection and Discrimination in Multi-terminal HVDC Grids and Potential Solutions

M. H. Naushath, A.D. Rajapakse

Abstract—By simulating a multi-terminal high voltage DC grid using a detailed electro-magnetic transient simulation model, challenges in fault detection and discrimination are demonstrated. To select the most appropriate signal for fast and reliable detection of faults, behavior of the DC grid during the faults is observed by means of various terminal measurements. By simulating different scenarios, challenging situations for discriminating faults in the protected line from the reverse faults, faults on the other pole, and from the remote breaker opening events are demonstrated. Influence of such disturbances on fault detection algorithms is evaluated and a method to discriminate faults in the protected line from the faults behind the relay is presented. Time taken to detect various faults in a typical high voltage DC grid is evaluated.

***Keywords*: Multi-Terminal HVDC (MT-HVDC), HVDC grid protection, HVDC Transmission line protection, DC side fault detection.**

I. Introduction

Multi-Terminal High Voltage Direct Current (MT-HVDC) transmission systems are being seriously considered as an alternative solution to overcome some of the limitations of HVAC power transmission systems. As voltage source convertor (VSC) technology facilitates to change the direction of power flow without changing the polarity of the voltage [1], the prospective HVDC technology for MT-HVDC grid is the VSC technology. The world's first VSC based three-terminal and five-terminal VSC-HVDC grids, respectively Nanao HVDC grid [2] and Zhoushan MT-HVDC [3], were placed in service respectively in 2013 and 2014. MT-HVDC grid proposals outside China include European Super Grid [4] and Atlantic Wind Connection [5]. To preserve the availability of the healthy part of MT-HVDC grid during DC side faults, an ultra-fast and reliable protection scheme is needed to clear DC side fault.

Lack of protection schemes that ensures smooth operation during DC side faults is considered as a major limitation in deploying MT-HVDC grids that are capable of continuing the operation during DC side faults. Any means of controlling fault current via reduction of DC side voltage, fault tolerant convertors such as those proposed in [6] are not suitable for large MT-HVDC as such strategies cause to cease operation of the whole grid via voltage collapsing. Therefore, DC circuit Breakers (DCCB) and DC disconnectors are proposed to clear DC side faults in MT-HVDC grids. To delay the time that fault current takes to reach the maximum breaker current, a small inductor is proposed to place in between the terminal and the breaker [1]. This terminal inductor significantly determines the behavior of measured voltage and current at the terminals during a DC side fault [1]. The fault indicator used in a protection scheme determines the speed of detection and capability to discriminate faults in the protected line from the faults in the adjacent lines. Due to limited speed and limited maximum DC breaking current, very fast fault detection scheme is needed for MT-HVDC grid protection.

The protection schemes that utilize fault current as the indicator can rely on differential current at two-terminals [7], estimated rate of rising fault current [8] or second order derivative of the fault current [9]. The methods that use the voltage or time rate of the voltage across the terminal inductor are alternative measures of first and second order time rate of fault current. As the line side voltage drops very rapidly during DC faults, the rate of change of line side voltage of the inductor [1] or rate of dropping line side voltage are a very commonly utilized fault indicators [10]-[11]. Although magnitude of drop in voltage or current magnitudes are not typically used as the main/sole indicator of faults, they are used as the supervisory conditions to improve the reliability [8], [10]. As measured voltage and current are indicators of faults, a zone of the trajectory in V-I plane can be used detect the fault as in [12]. The ratio between frequency components within 1 kHz-5 kHz of the line side voltage to the terminal voltage is used in [13] to detect faults. The magnitude of this fault indicator reflects the direction of the fault. Energy based methods proposed for LCC-HVDC systems such as [14] uses voltage and current measurements at both ends to discriminate internal faults from the external faults. Therefore, time to detect the fault depends on speed of changing voltage and current. However, any protection scheme which includes communication is not a likely to be satisfactory for MT-HVDC grids as communication delays may not be tolerated. The presence of backward travelling waves is an indicator of a fault. Therefore, magnitude of the backward travelling wave is compared with a threshold level to detect faults in protections schemes proposed for LCC-HVDC [15], [16]. In terms of basic measurements, such travelling wave based methods can be considered as a system utilized both voltage and current measurements as backward travelling wave E_b is evaluated by

$$E_b = \Delta V_T - Z\Delta I_T \quad (1)$$

M. H. Naushath & A. D. Rajapakse are with the Department of Electrical & Computer Eng., University of Manitoba, Winnipeg, MB, Canada, R3T5V6 (email: umnausha@myumanitoba.ca, Athula.Rajapakse@umanitoba.ca)

Paper submitted to the International Conference on Power Systems Transients (IPST2017) in Seoul, Republic of Korea June 26-29, 2017

Common protection challenges include fault discrimination, detecting high resistance faults, speed, and reliability of fault detection. Fault discrimination challenges includes discriminating fault transients in the protected line from faults in adjacent lines, faults in the other pole (in case of bi-pole transmission), and transients caused by breaker operations in adjacent lines. This paper will investigate some of the above issues through electro-magnetic transient simulation. As challenges and performance depend on the type of protection scheme, four basic fault detection schemes relying on four distinct measurements are investigated. Solutions for mitigating some of the problems will be proposed.

II. Simulation Case

Electro-magnetic transient simulation model of the test grid shown in Fig. 1 is developed to demonstrate the DC side fault behavior. To investigate different type of contingencies, a bipolar MT-HVDC grid consisting of both short and long underground cables and overhead lines are added. Longs lines are important to investigate challenges in detecting high resistance remote faults while short lines are important to understand the problems that may arise due to short wave travel times, and sharp wave fronts. Frequency depended transmission line and cable models in PSCAD are used for accurate estimation of the transient behavior.

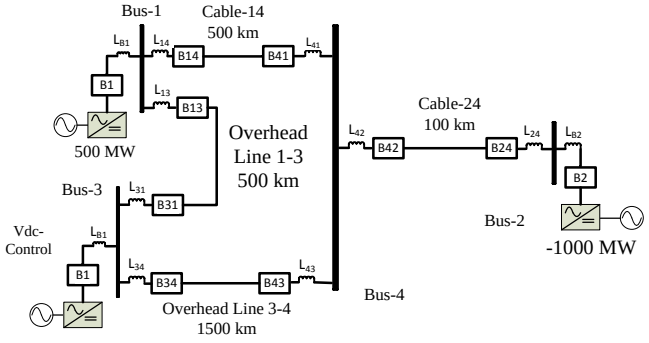

Fig. 1. Bipole-HVDC test grid

The metallic return wire having a single ground at Bus-3 (with a low resistance of 0.05Ω) is used. The MMCs connected to Buses-1, 2 and 3 were modeled with decoupled controls and converter transformers. The basic data of the grid is given in Table-I.

TABLE I: Test Grid Details

Parameter	Value	Units
Nominal AC Voltage (V_{LL})	230	kV
Nominal DC Voltage	±320	kV
Equivalent MMC DC Capacitance	100	μF
Number of levels	98	-
di/dt limiting reactor L_{xy}	30	mH
di/dt limiting reactor L_{Bx}	15	mH
Nominal DC Grid Power	1,000	MW

Terminal inductors, which are placed between the transmission line and a bus, lower the rate of rise of fault currents to allow sufficient time for the DC circuit breakers to interrupt the fault current. Although the value of terminal inductors is mainly dictated by the DC breaker capability and the grid characteristics, it is a factor that has very high influence on the capability of discriminating faults on different zones [1]. Discriminating faults in the protected line from adjacent lines is easy with larger inductor and also gives more time to isolate faults. However, larger inductors are more expensive, require larger space, raise the amount of energy to dissipate through MOV during fault current interruption, and can cause instabilities in convertor control [17]. With the aim of investigating a more realistic situation, a 30 mH inductor is used between each transmission line and the bus.

Fault on the converter bus can be cleared using a DCCB or by de-energizing the converter using AC circuit breaker. As it will be shown later, the two schemes exhibit significantly different fault transients at a converter bus. Therefore, two versions: (i) Scheme-1 which uses ACCB to shut-down VSC at bus faults [9],[10],[11], and (ii) Scheme-2 which has a DCCB (and a 15 mH series inductor) between the converter and the bus to clear converter bus faults [8] are considered.

The impact of limited sensor band width and sampling process in signal processing circuit is mimicked by taking measurements through a 12.5 kHz low pass filter and the band limited signal is sampled at 50 kHz. The grid is simulated at small time step of 10 μs. Quantization error caused by a 16 bits analogue-to-digital conversion is modeled.

III. Fault Behavior and Fault Detection Challenges

A. *Transient Behavior at a DC side Fault*

Understanding transient behavior of the terminal measurements is important in selecting the suitable input signals for fault detection. Potential measurements of a relay located at a terminal include (say relay RXYP on Positive-pole of terminal X protecting line XY) the terminal current (I_{XYP}), the line side voltage (V_{XYP}) of the inductor L_{XYP}, voltage across the inductor (V_{LXYP}), and the bus voltage V_{XP}. Fig. 2 shows an example of the above signals. They were observed at relay R14P located at DCCB B14 during a solid P-pole to ground fault (P→G) on Cable-14 for scheme-1.

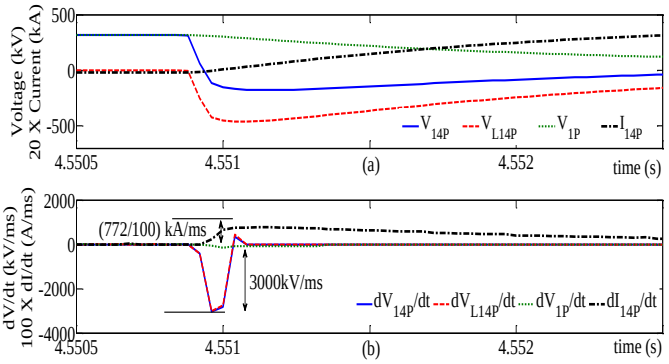

Fig. 2. Measurements during a 0.01Ω P→G fault on C14, 100km away from R14 for Scheme-1 (a) P-pole voltages and currents, (b) peak dv/dt

For the clarity of illustration, current I_{14N} is scaled up by a

factor of 20 in Fig 2. According to Fig. 2 (a), V_{14P} and V_{L14P} drop very rapidly. The rate of change of voltage (ROCOV) values appears as sharp spikes and ROCOV based fault detection algorithms trigger once the estimated ROCOV exceeds the threshold. ROCOV value of V_{1N} is much smaller than ROCOV values of V_{14P} and V_{L14P}. The influence of inductor value on ROCOV value is discussed in [1]. Furthermore, the fault current rises continuously as I_{14P} is the time integral of voltage V_{L14P}.

$$I_{14P} = \frac{1}{L_{14}} \int V_{L14P}\, dt \tag{2}$$

As depicted in Fig. 2 (a), the peak rate of change of current (7.72 kA/ms) is much smaller than the initial ROCOV values (3000 kV/ms) of voltages. Therefore, current magnitude based fault detection takes longer time to detect faults. For Scheme-1, as depicted in Fig. 2 (b), rate of changing V_{14P} and V_{L14P} are almost the same in magnitude as the change in V_{1P} is much slower than V_{14P}. Therefore, fault detection based on V_{14P} or V_{L14P} are almost identical for Scheme-1. However, as depicted in Fig. 3, a significant change in magnitude and ROCOV of V_{1P} is resulted by a DC side fault in Scheme-2.

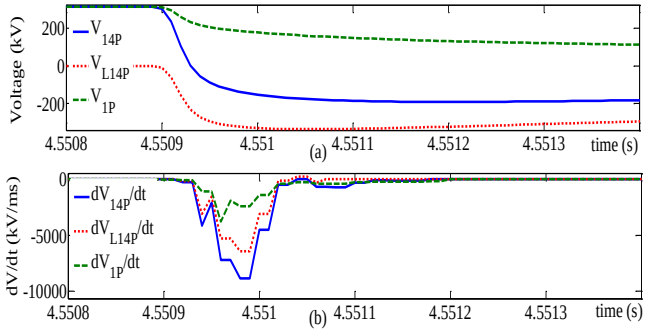

Fig. 3. Measurements during a 0.01Ω P→G fault on C14, 100km away from R14 for Scheme-2 (a) P-pole voltages and currents, (b) peak dv/dt

In order to show how challenging the DC side fault current interruption in a typical MT-HVDC grid, the transient behavior of the fault current observed at the R14N and R41N are shown in Fig. 4 in large time scale for near and far end solid faults. In Fig. 4, l_f is the distance between the fault and the relay and t_f is the fault inception time. Furthermore, rate of rising fault current at R41N is lower than R14N due to larger total series inductance/resistance between the fault and the source behind it.

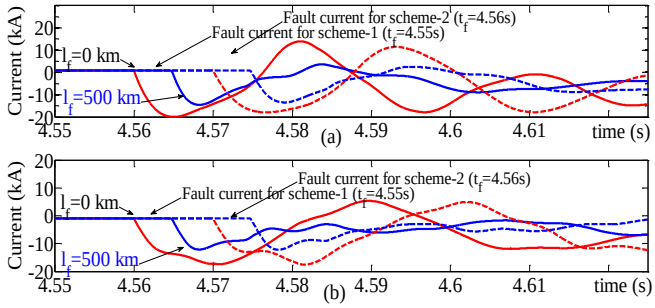

Fig. 4. Fault current transients for scheme-1 (t_f=4.55s) and scheme-1 (t_f=4.56s) during 0.01Ω N→G fault on Cable-14 (a) at R14N, (b) at R41N

B. *Sensitivity/Highest Detectable Fault Resistance*

DC side fault detection scheme should be able to detect and discriminate faults before the fault current rises above the DCCB capacity, typically in several milliseconds. The fault detection scheme should be sensitive enough to fast detect the faults which can cause steady state fault currents above the DCCB current rating. For example when using a 10kA DCCB in a ±320 kV scheme, up to 32Ω high resistance pole-ground faults or up to 64 Ω high resistance pole-to-pole faults need to be detected in a few milliseconds. The different fault indicators discussed in Section III-A can be compared in terms of the sensitivity to high resistance faults. The four fault indicators chosen are: (A) peak [$dV_{XYN,P}/dt$], (B) peak [$dV_{XYLN,P}/dt$], (C) peak [$V_{XYLN,P}$], and (D) [$V_{14N,P}/V_{1N,P}$]* (*band limited to 1 kHz-5 kHz) as in [13]. However, no window is used for Method-D as in [13]. Furthermore, voltage across the inductor is used instead of dI/dt as it is an implicit measure of dI/dt. Therefore, first three methods are the basis of most of the fault detection schemes proposed in literature.

An independent line protection schemes on each pole is assumed and the threshold for each fault indicator is set at 140% of the peak value of the respective signal observed for a short circuit at the remote bus in the forward direction. This allows discrimination of faults on the remote bus zone from the line faults. It is assumed that a way of detecting direction of the fault is available, and thus the effect of reverse faults is ignored in this analysis. To determine the sensitivity, detectability of high resistance faults at the remote end of the protected line is evaluated. Table-II shows the estimated settings for relays R14N (protecting Cable 1-4) and R34N (protecting O/H line 3-4) for the tripping Schemes 1 and 2. The sensitivity, expressed as the maximum resistance of the N →G fault applied at the remote end which is detectable by the relay, is found for each method and compared in Table-III.

TABLE II: SETTINGS FOR R14N AND R34N

Fault detection method	Scheme-1 @R14		Scheme-2@R14	
	Peak disturbance	R14 Setting Scheme-1	Peak disturbance	R14 Setting scheme-2
Meth. A	109.8 kV/ms	154 kV/ms	119 kV/ms	167 kV/ms
Meth. B	91.5 kV/ms	128 kV/ms	64 kV/ms	90 kV/ms
Meth. C	-114 kV	-160 kV	-96.6 kV	-135kV
Meth. D	11.3	15.8	8.0	11.3
	Peak disturbance	R34 Setting for scheme-1	Peak disturbance	R34 Setting for scheme-2
Meth. A	1483 kV/ms	2077 kV/ms	1647 kV/ms	2059kV/ms
Meth. B	1483 kV/ms	2077 kV/ms	1199kV/ms	1499kV/ms
Meth. C	-149 kV	-186 kV	-125kV	-157kV
Meth. D	570	712	59	73.75

TABLE III: SENSITIVITY OF R14N & R34N

Scheme	Maximum Detectable Fault Resistance (Ω) @R14N			
	Meth.-A	Meth.-B	Meth.-C	Meth. D
Sc-1	89	106	7	435
Sc-2	80	99	5	52
	Maximum Detectable Fault Resistance (Ω) @R34N			
Sc-1	107	107	53	0
Sc-2	103	102	19	0

When applied to detect the faults in *cables*: (i) Method-C is the least sensitive one and only capable of detecting faults having resistance up to 5 or 7 Ω, (ii) sensitivity of Method-D significantly drops when used with Scheme-2, (iii) Method-A and B have comparable sensitivities and capable of detecting faults having less than 4 kA steady state currents.

When applied to detect the faults in *overhead transmission lines:* (i) faults having higher resistance could be detected even with longer overhead lines using Methods A, B, C (O/H line OHL-34 is 1500km long compared to Cable C-14 of 500 km), (ii) Method-D fails as the observed ratio between the line side voltage to bus voltage for a solid fault at the end of the line is less than the settings, regardless of the tripping scheme. However, in order to detect high resistance faults beyond 100Ω, a communication based scheme such as current differential or overcurrent magnitude based fault detection scheme can be used as the backup protection scheme. Furthermore, bus fault detection is not so much challenging as current differential protection can be applied without any overhead on delay for communication.

C. Discriminating Faults in Other Lines and Pole

The ability of discriminating the faults on adjacent lines from those on the protected line is dependent on type of the bus (converter bus, ex. bus-1, 2, and 3 or intermediate bus, ex. bus-4) at the relay location and the type of transmission line (cable or O/H line). Fig. 5 compares (i) the signals observed by R14N during a reverse fault (short cct. on OHL-31, 50 km away from bus-1) with (ii) the signals observed by R13N for a reverse fault (short cct. on Cable-14, 50km away from bus-1).

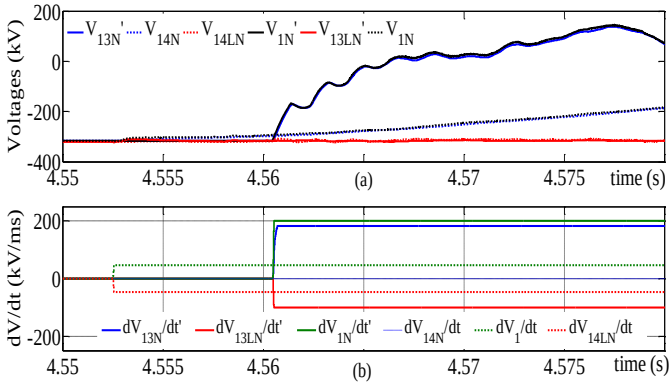

Fig. 5. Signal observed by R14N and R13N during solid N→G reverse faults for Scheme-1 (a) voltages (b) output of a peak dV/dt detector

According to Fig. 5, transient observed by OHL relay R13N during the reverse cable fault is much stronger than the transient observed by cable relay R14N during the reverse overhead line fault. Fig. 6 shows the same quantities when Scheme-2 is used. Compared to the case of Scheme-1, very fast transients are observed by both relays (R31N and R41N) for the reverse faults on adjacent lines. Therefore, discriminating the faults is much challenging if Scheme-2 is used. On the other hand, adjacent relay is almost undisturbed under scheme-1 as the bus is directly connected to the converter. For the same reason, fault discrimination is more challenging in intermediate buses such as bus-4 compared to converter buses.

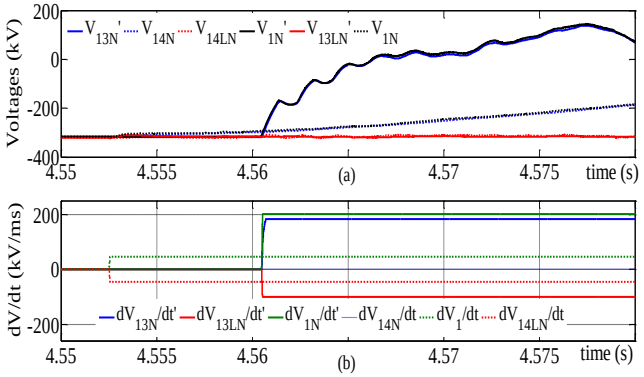

Fig. 6. Signal observed by R14N and R13N during solid N→G reverse faults for Scheme-2 (a) voltages (b) output of a peak dV/dt detector

Another issue is the induced transients due to mutual coupling, depicted in Fig. 7. An abrupt transient occurs in N-pole voltages during a fault on P-pole. This transient creates a significant ROCOV value which may generates trip signal for N-pole protection scheme.

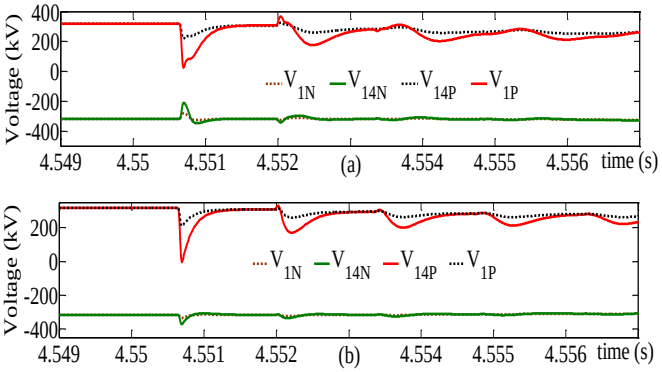

Fig. 7. Observed transients in N-pole during faults on P-pole at 200 km away from R43N (a) voltage for P→G faults (b) voltages for P→R faults

Table-IV shows measured disturbances at R43N, during reverse bus faults (solid N→G and N→R faults) and faults on the other pole (solid P→G and P→R faults).

TABLE IV: DISTURBANCE AT R43N FOR SCHEME-2

Event	Location	peak [dV_{43N}/dt] (kV/ms)	peak [dV_{43LN}/dt] (kV/ms)	peak [V_{43LN}] (kV)	V_{43N}/V_{4N}
N→G	Bus-3	1666	1098	-118	16
N→R	Bus-4	2664	-6161	246	23.7
N→G	Bus-4	2590	-6088	242	263.0
N→G*	Bus-4	2618	-6042	242	23.7
P→R	0km @O43	-1208	-796	34	4.7
P→R	200km @O43	-1254	-823	36	7.0
P→G	0km @O43	-1254	-833	36	6.5
P→G*	0km @O43	-1245	-833	36	6.5
P→G	50km @O43	1464	979	40	5.0
P→G	200km @O43	2462	1629	-60	5.0

Where O43 is the overhead transmission line connecting Bus-4 and Bus-3. Table-V shows measured disturbances at R41N. Since the converter inductor L_{B3} has no significant

effect on relays at bus-3, only scheme-2 is considered here. The symbol "*" indicates observations taken after reversing the direction of power flow.

TABLE V: DISTURBANCE AT R41N FOR SCHEME-2

Event	Loc.	peak [dV_{41N}/dt] (kV/ms)	peak [dV_{41LN}/dt] (kV/ms)	peak [V_{41LN}] (kV)	V_{41N}/ V_{4N}
N→G	Bus-1	119	55	-80	8
N→R	Bus-4	137	-7360	332	7.6
N→G	Bus-4	146	-7461	341	4.0
N→G*	Bus-4	138	-7461	341	4.0
P→R	0km @C14	0	-137	34	4.6
P→R	200km @ C14	0	-64	39	6.0
P→G	0km @ C14	0	45	-36	3.8
P→G	200km @ C14	0	37	-34	3.5
P→G*	0km @ C14	0	46	-36	4.0

where C14 is the cable connecting Bus-1 and Bus-4. Observed disturbance during a solid fault on the forward remote bus is shown in the first raw as a reference for comparison. According to Table-IV and Table-V, a relay at an intermediate bus cannot set by considering the disturbance for a forward direction remote bus fault, especially in the cases of peak [dV_{XYLN}/dt] and peak [V_{XYLN}] based fault detection, unless there is means to detect the direction of the fault with respect to the relay. However, the sign of the peak [dV_{XYLN}/dt] and peak [V_{XYLN}] is dependent on the direction of fault, and can be easily used to discriminate forward faults in the protected line from the reverse faults.

According Table-V, there is no significant impact from the P-pole faults on the N-pole relays based on peak [dV_{XYN}/dt] in the case of cables. However, according to Table-IV, high ROCOV values can be observed in N-pole voltages of the O/H line during P-pole faults. This is expected as there is more mutual coupling in O/H lines, and therefore, a faulty pole identification method is required for bi-pole O/H lines.

D. Discriminating Faults Transients from Remote Breaker Opening Transients

Breaker opening causes a strong transient on the adjacent and remote relay locations. This can induce false tripping and undesirable interruption of power flow in the healthy parts of the grid. Table-VI compares the disturbances observed at R43N due to opening of remote breakers. For comparison purpose, observation during the forward remote bus fault (used for setting) is shown in the first raw. The symbols '*' and ' ' ' represent the observed disturbance after reversing the power and reducing the power level to half, respectively.

According to Table VI, the sign of the ROCOV value depends on the direction of power flow and some breaker opening transients can be discriminated from the faults as they create transients with opposite polarity to fault transients. Although the simulated DCCB does not model individual semiconductor switching devices in detail, it captures the essential features of the hybrid DCCB described in [18] (fast mechanical switch, IGBT switch, and MOV), which are relevant for the system level studies. The same approach used in references [19] in modelling the DCCB is used in this paper.

TABLE VI: DISTURBANCE OBSERVED DURING REMOTE BREAKER OPENING AT R43N (FOR SCHEME-2)

Breaker	peak [dV_{43N}/dt] (kV/ms)	peak [dV_{43LN}/dt] (kV/ms)	peak [V_{43LN}] (kV)	V_{43N}/ V_{4N}
	1666	1098	-118	16
B41-N	-1309	3048	-124	7.0
B41-N*	1309	-3057	125	35.1
B41-N'	-1254	2957	-118	38
B42-N	1336	-3103	127	8.3
B34-N	-979	-640	49	4.5
B31-N	165	110	-9	3.7
B41-P	-219	-137	22	6.1
B42-P	0	-73	7	1.7

However, according to Table-VII, breaker opening creates a severe impact on the relays protecting overhead transmission lines. Note that opening of the breakers connected to the same bus creates the highest disturbance, however, local signal based blocking schemes can be used avoid false tripping, as these relays a physically close.

TABLE VII: DISTURBANCE OBSERVED DURING REMOTE BREAKER OPENING AT R41N (FOR SCHEME-2)

Breaker	peak [dV_{41N}/dt] (kV/ms)	peak [dV_{41LN}/dt] (kV/ms)	peak [V_{41LN}] (kV)	V_{41N}/ V_{4N}
	119	55	-80	8
B42-N	73	-3808	170	0.8
B43-N	-37	2838	-125	5
B14-N	-37	-18	6	6

E. Time to Detect Faults

The Most challenging issue in MT-HVDC grid protection is the prompt to detection of DC side faults and interruption of fault currents before exceeding the breaker capacity. Table-VIII and Table-IX compare the times taken to detect faults by R14N and R34N.

TABLE VIII: FAULT DETECTION TIME OF R14N

Loc. (km)	$T_{Critical}$ (ms)		Time taken to detect faults (μs)							
			Meth.-A		Meth.-B		Meth.-C		Meth.-D	
	Sc-1	Sc-2	Sc-1	Sc-2	Sc-1	Sc-2	Sc-1	Sc-2	Sc-1	Sc-2
0	1.32	1.98	20	20	20	20	40	40	20	220
100	1.74	2.11	107	97	107	97	127	127	107	347
250	3.37	3.81	237	237	237	237	297	297	257	517
500	6.20	6.77	453	453	453	453	613	653	493	813

Fault detection time $T_{Detection}$ is estimated as:

$$T_{Detection} = T_{Trip} - len \cdot \times V_{Travel} - T_{Fault\_inception} \quad (4)$$

where T_{Trip} is the time when the algorithm sets output, *len* is the length between the relay and the fault location, V_{Travel} is the propagation velocity in the considered transmission line, $T_{Fault\_Inception}$ is the time when fault is applied. The estimated velocity of propagation is 120 km/ms for the cable and 300 km/ms for the overhead transmission line. The symbol α indicates that the maximum fault current never exceeds the breaker capacity. The symbol 'x' indicates that fail to detect the fault. The rate of rise of fault current is lower in Scheme-2 than Scheme-1 (and therefore results a smaller peak fault

current) due to larger total series inductance.

TABLE XI: FAULT DETECTION TIME OF R34N

Loc. (km)	$T_{Critical}$ (ms)		Time taken to detect faults (μs)							
			Meth.-A		Meth.-B		Meth.-C		Meth.-D	
	Sc-1	Sc-2	Sc-1	Sc-2	Sc-1	Sc-2	Sc-1	Sc-2	Sc-1	Sc-2
0	1.02	1.46	40	40	40	40	60	60	120	220
250	17.73	18.7	27	27	27	27	67	67	107	x
750	191	191.6	40	60	40	60	80	100	x	5760
1500	α	α	80	80	80	80	100	120	x	x

The maximum time taken to detect faults as a fraction of the time available to interrupt the fault current (for a 10 kA DCCB) is as small as 0.04 for Methods-A and B. However, for the considered operating voltage and the terminal inductor value, an ultra-fast DCCB that can interrupt 10 kA fault current within 1 ms is required. But, if the inductor values are doubled (L_{XYN}=60 mH and L_{BX}=30 mH), a DCCB capable of interrupting 10 kA within 3 ms can be used as can be seen from Table-X. These inductor values are still significantly smaller than the inductors used in some other studies (for example a 200mH inductor used in [9]), but they can increase the energy dissipation in MOV during fault current interruption up to 4.5MJ (calculated using ½ LI^2 at I= 10 kA). This value is comparable with the energy dissipated in 9kA breaker tested with 100mH inductor in [18].

TABLE X: FAULT DETECTION TIMES OF R34N WITH A LARGER INDUCTOR

Loc. (km)	$T_{Critical}$ (ms)	Time taken to detect faults (μs) @R34 scheme-2			
		Meth.-A	Meth.-B	Meth.-C	Meth.-D
0	3.02	40	40	60	x
250	21.38	17	17	67	x
750	193.5	40	40	80	x

IV. CONCLUSIONS

The ROCOV based fault detection methods that utilizes line side voltage or voltage across the terminal inductors are more sensitive than the current gradient based or current magnitude based fault detection. Such ROCOV based fault detection schemes are capable of detecting faults which cause less than 4 kA in the test grid studied. High resistance faults that cause fault currents less than 4 kA can tolerate a slower backup fault detection scheme such as current differential fault detection. Discriminating faults in the protected line from the reverse faults is challenging, especially in the cases of O/H transmission lines and the relays located at buses which are not directly connected to a VSC. However, polarity of the inductor voltage during the fault transient can be used to discriminate side of the fault with respect to the relay. Although faults on a cable connected to one pole do not create a significantly high transient on the other pole, a significant voltage transient can be observed on the healthy pole of an overhead transmission line. ROCOV based fault detection schemes are very fast and the maximum detection times are only a tiny fraction of the time available for breaking the fault current. However, for a small terminal inductor value such as 30 mH, fault currents grow very rapidly during DC side faults. To overcome this challenge, larger terminal inductors, VSC controllers which are stable under larger series inductors, and fast DCCBs are required.

V. REFERENCES

[1] J. Sneath and A. D. Rajapakse, "Fault Detection and Interruption in an Earthed HVDC Grid Using ROCOV and Hybrid DC Breakers," in IEEE Trans. on Power Delivery, vol. 31, no. 3, pp. 973-981, June 2016.

[2] X. Li, Z. Yuan, J. Fu, Y. Wang, T. Liu and Z. Zhu, "Nanao multi-terminal VSC-HVDC project for integrating large-scale wind generation," IEEE PES General Meeting, National Harbor, MD, 2014, pp. 1-5.

[3] Z. Jie, L. Haibin, X. Rui, N. Wenhai, S. Kun, H. Feiyang, L. Dapeng, "Research of DC circuit breaker applied on Zhoushan multi-terminal VSC-HVDC project," IEEE PES Asia-Pacific Power and Energy Engineering Conference (APPEEC), Xi'an, 2016, pp. 1636-1640.

[4] D. Van Hertem and M. Ghandhari, "Multi-terminal VSC HVDC for the European supergrid: Obstacles," Renewable and Sustainable Energy Reviews, vol. 14, no. 9, pp. 3156–3163, Dec. 2010.

[5] G. D. Irwin, A. Isaacs, and D. Woodford, "Simulation requirements for the Atlantic Wind Multi-Terminal VSC Offshore Wind Project," in Proc. IEEE T&D Conf. and Exposition, pp. 1–4, May 2012

[6] M. M. Merlin, T. C. Green, P. D. Mitcheson, D. Trainer, R. Critchley, W. Crookes, F. Hassan, "The Alternate Arm Converter: A New Hybrid Multilevel Converter With DC-Fault Blocking Capability," in IEEE Trans. on Power Delivery, vol. 29, no. 1, pp. 310-317, Feb. 2014.

[7] M. Hajian, L. Zhang and D. Jovcic, "DC Transmission Grid With Low-Speed Protection Using Mechanical DC Circuit Breakers," in IEEE Trans. on Power Delivery, vol. 30, no. 3, pp. 1383-1391, June 2015.

[8] S. Pirooz Azad; D. Van Hertem, "A Fast Local Bus Current-Based Primary Relaying Algorithm for HVDC Grids," in IEEE Trans. on Power Delivery , vol.PP, no.99, pp.1-1

[9] R. Li; L. Xu; L. Yao, "DC Fault Detection and Location in Meshed Multi-terminal HVDC Systems Based on DC Reactor Voltage Change Rate," in IEEE Trans. on Power Delivery , vol.PP, no.99, pp.1-1

[10] W. Leterme, J. Beerten and D. Van Hertem, "Nonunit Protection of HVDC Grids With Inductive DC Cable Termination," in IEEE Trans. on Power Delivery, vol. 31, no. 2, pp. 820-828, April 2016.

[11] F. Kong, Z. Hao and B. Zhang, "A Novel Traveling-Wave-Based Main Protection Scheme for \pm 800 kV UHVDC Bipolar Transmission Lines," in IEEE Trans. on Power Delivery, vol. 31, no. 5, pp. 2159-2168, Oct. 2016.A.

[12] W. Leterme, S. Pirooz Azad and D. Van Hertem, "A Local Backup Protection Algorithm for HVDC Grids," in IEEE Trans. on Power Delivery, vol. 31, no. 4, pp. 1767-1775, Aug. 2016.

[13] J. Liu; N. Tai; C. Fan, "Transient-Voltage Based Protection Scheme for DC Line Faults in Multi-terminal VSC-HVDC System," in IEEE Trans. on Power Delivery , vol.PP, no.99, pp.1-1.

[14] Zheng, T. Nengling, Y. Guangliang and D. Haoyin, "A Transient Protection Scheme for HVDC Transmission Line," in IEEE Trans. on Power Delivery, vol. 27, no. 2, pp. 718-724, April 2012.

[15] Y. Zhang, N. Tai and B. Xu, "Fault Analysis and Traveling-Wave Protection Scheme for Bipolar HVDC Lines," in IEEE Trans. on Power Delivery, vol. 27, no. 3, pp. 1583-1591, July 2012.

[16] J. Wu; H. Li; G. Wang; Y. Liang, "An Improved Travelling Wave Protection Scheme for LCC-HVDC Transmission Lines," in IEEE Trans. on Power Delivery , vol.PP, no.99, pp.1-1.

[17] W. Wang, M. Barnes, O. Marjanovic and O. Cwikowski, "Impact of DC Breaker Systems on Multiterminal VSC-HVDC Stability," in IEEE Trans. on Power Del., vol. 31, no. 2, pp. 769-779, April 2016.

[18] Häfner J., Jacobson B.: 'Proactive Hybrid HVDC breakers - A key innovation for Reliable HVDC grid'. Cigré symposium, Bologna, Italy, Sept. 2011.

[19] M. Hajian, D. Jovcic and B. Wu, "Evaluation of Semiconductor Based Methods for Fault Isolation on High Voltage DC Grids," in IEEE Transactions on Smart Grid, vol. 4, no. 2, pp. 1171-1179, June 2013.